Journal of Magnetic Resonance 205 (2010) 276–285

Contents lists available at ScienceDirect

Journal of Magnetic Resonance

journal homepage: www.elsevier.com/locate/jmr

Extended phase graphs with anisotropic diffusion

M. Weigel [a,*], S. Schwenk [a], V.G. Kiselev [a], K. Scheffler [b], J. Hennig [a]

[a] University Hospital Freiburg, Department of Radiology, Medical Physics, Breisacher Strasse 60a, 79106 Freiburg, Germany
[b] University of Basel Hospital, Department of Radiology, Division of Radiological Physics, Petersgraben 4, 4031 Basel, Switzerland

ARTICLE INFO

Article history:
Received 9 January 2010
Revised 17 May 2010
Available online 12 June 2010

Keywords:
Extended phase graph
EPG
Diffusion
Anisotropy
Diffusion coefficient
Diffusion tensor
Diffusion weighted imaging
Multi-pulse
RARE
TSE
FSE

ABSTRACT

The extended phase graph (EPG) calculus gives an elegant pictorial description of magnetization response in multi-pulse MR sequences. The use of the EPG calculus enables a high computational efficiency for the quantitation of echo intensities even for complex sequences with multiple refocusing pulses with arbitrary flip angles. In this work, the EPG concept dealing with RF pulses with arbitrary flip angles and phases is extended to account for anisotropic diffusion in the presence of arbitrary varying gradients. The diffusion effect can be expressed by specific diffusion weightings of individual magnetization pathways. This can be represented as an action of a linear operator on the magnetization state. The algorithm allows easy integration of diffusion anisotropy effects. The formalism is validated on known examples from literature and used to calculate the effective diffusion weighting in multi-echo sequences with arbitrary refocusing flip angles.

1. Introduction

The extended phase graph (EPG) [1–3] calculus describes the response of magnetization in Fourier space. As such it is related to the *k*-space concept used to describe spatial encoding [4–6]. It can be understood as a solution of the Bloch equation [7] using its Fourier representation and is especially well suited for the characterization of spin systems that are strongly dephased by magnetic field inhomogeneities or switched gradients [1–3,8]. Instead of tracing different phase evolutions of spins, the spin system is depicted by a finite set of phase state constellations [1–3,8]. The EPG of an MR sequence can then be calculated stepwise using a transition matrix formalism between specific points of interest, e.g. from RF pulse to RF pulse or from RF pulse to echo or equivalent [1,2]. This allows for a more intuitive and pictorial understanding of echo formation and assignment.

MR sequences are described by consecutive events of RF pulses, switched magnetic field gradients, and free phase evolution [2,8]. For understanding the generic response of multi-pulse sequences, a one-dimensional (1D) dephasing coordinate is normally sufficient, and the intricacies of *k*-space trajectories are ignored. This allows to include T_1- and T_2-relaxation effects, which are independent of the actual *k*-space trajectory of transverse magnetization pathways. Diffusion and flow effects depend on the timing and amplitude of the gradients used and are therefore neglected [1–3,8].

Explicit analytical expressions for the echo amplitudes of multi-pulse sequences were also published, based on a generating function formalism [9,10]. However, diffusion and flow effects are neglected as well.

Progress in quantifying diffusion and flow effects of multi-spin echo sequences has been made by Kiselev [11]. The Bloch–Torrey equation [12] was solved in Fourier space with account for the diffusion and flow effects. The solution was built as a chain of operators acting on the Fourier transform of the magnetization. Calculations were performed for isotropic diffusion and piece-wise constant gradient applied in a single direction, but omitting the explicit formula for the diffusion operator [11]. Similar results were obtained by Zur [13] who used the spinor technique and briefly discussed the diffusion anisotropy. A phenomenological description of flow within the 1D EPG was also published [14].

The purpose of this work is to introduce diffusion effects into the framework of the EPG algorithm to allow for a simplified description of these effects in sequences with multiple, arbitrary RF pulses, particularly the CPMG sequence [15,16]. In order to account for diffusion anisotropy the EPG formalism is extended

* Corresponding author. Fax: +49 761 270 3831.
E-mail addresses: Matthias.Weigel@uniklinik-freiburg.de (M. Weigel), Stefanie.Schwenk@uniklinik-freiburg.de (S. Schwenk), Valerij.Kiselev@uniklinik-freiburg.de (V.G. Kiselev), Klaus.Scheffler@unibas.ch (K. Scheffler), Juergen.Hennig@uniklinik-freiburg.de (J. Hennig).

1090-7807/$ - see front matter © 2010 Elsevier Inc. All rights reserved.
doi:10.1016/j.jmr.2010.05.011

to include all three dimensions covered by the spatial coordinates of the gradient system. The time course of all three gradient components is independent and can be arbitrary. For verification and illustration of the formalism, the obtained result of an anisotropic diffusion operator is applied to both basic examples to demonstrate and verify the formalism with already known solutions and more complex, new examples to present and underline its potential.

2. Theory

2.1. Extended phase graphs in three dimensions

The fundamental Bloch equation is defined in three-dimensional position space (x-space) with $\mathbf{r} = [x,y,z]^\dagger$ to depict magnetization as a vector with the components $\mathbf{M} = [M_x,M_y,M_z]^\dagger$. $\mathbf{M}$ depends on the spatial coordinates and evolves with time: $\mathbf{M}(\mathbf{r},t)$. The symbol "†" denotes the Hermitian conjugation of vectors and matrices throughout this text.

MR imaging sequences use many gradient steps for spatial encoding, which results in dephased magnetization constellations during most of the time of the sequence. Dealing with dephased magnetization (in x-space), however, is an extensive task using the Bloch equation, which requires calculations over a multitude of spins. The characterization of dephased spin states used by the EPG is much more simple and is based on the Fourier space coordinate $\mathbf{k}$ [6]:

$$k_n(t) = \gamma \int_{t'=0}^{t} G_n(t')dt' = \int_{t'=0}^{t} g_n(t')dt', \tag{1}$$

where $n = x, y, z$ and the common substitution $\mathbf{g} = \gamma\mathbf{G}$ was made. Eq. (1) introduces with $\mathbf{k} = [k_x,k_y,k_z]^\dagger$ a quantitative measure of dephasing of the whole spin system with three-dimensional (3D) dephasing coordinates due to acting arbitrary gradients $\mathbf{G}(t) = [G_x,G_y,G_z]^\dagger$.

In the Fourier based EPG calculus magnetization is represented by the corresponding Fourier transforms:

$$F_+(\mathbf{k}) = \int_V \{M_x(\mathbf{r}) + iM_y(\mathbf{r})\} \exp(-i\mathbf{kr})d^3r, \tag{2}$$

$$F_-(\mathbf{k}) = \int_V \{M_x(\mathbf{r}) - iM_y(\mathbf{r})\} \exp(-i\mathbf{kr})d^3r, \tag{3}$$

$$Z(\mathbf{k}) = \int_V M_z(\mathbf{r}) \exp(-i\mathbf{kr})d^3r, \tag{4}$$

where all integrations are performed over the macroscopically large sample volume. Basic properties of the Fourier transform lead to the additional relations $F_+^*(\mathbf{k}) = F_-(-\mathbf{k})$ (definition of $F_\pm$) and $Z(-\mathbf{k}) = Z^*(\mathbf{k})$ (M_z is real), with "$*$" signifying the complex conjugate.

Eqs. (2) and (3) use a slightly different notation compared to the original publications [1–3] to be mathematically more rigorous. They represent the general continuous form of the EPG. Especially for regular and periodic MR sequences such as RARE (TSE, FSE) [17] or TrueFISP (balanced SSFP) [18,19] only a discrete set of $\mathbf{k}$-values and, hence, $F_\pm(\mathbf{k})$- and $Z(\mathbf{k})$-values is generated. These are called phase states or partition states.

The complete magnetization constellation of a spin system at a given time is usually described by a vector $\mathbf{F}$ of various EPG partition states with different $\mathbf{k}$ (representation in 3D):

$$\mathbf{F} = \left(F_{\mathbf{k}_0}F_{\mathbf{k}_1}F_{\mathbf{k}_2}F_{\mathbf{k}_3}\cdots Z_{\mathbf{k}_4}Z_{\mathbf{k}_5}Z_{\mathbf{k}_6}\cdots\right)^{\mathrm{T}}. \tag{5}$$

Generally, the number of elements in $\mathbf{F}$ changes with time, since RF pulses can create EPG states or combine EPG states, and relaxation and diffusion effects can eliminate EPG states [1–3]. From a more rigorous physical point of view, it may be more appropriate to claim that $\mathbf{F}$ theoretically contains all possible EPG states that the examined sequence can access, but only a very small minority of them has a non-vanishing population, meaning a Fourier component that is not 0. Then, the creation of an EPG state means that its corresponding population becomes unequal 0, the elimination of an EPG state means that its population assumes 0.

Clearly for practical reasons, $\mathbf{F}$ will always only contain the non-vanishing partition states within this text.

In a typical one-dimensional EPG representation for periodic sequences $\mathbf{F}$ could look like the following:

$$\mathbf{F} = (F_0Z_0F_1F_{-1}Z_1F_2F_{-2}Z_2\cdots F_{+k}F_{-k}Z_k)^{\mathrm{T}}. \tag{6}$$

The later presented examples below will make use of the vector $\mathbf{F}$ similar to the form presented above.

A summary of the currently published operators solved for the EPG calculus (1D-representation) is as follows [1–3,8,11]:

- *Shift operator $\mathcal{S}$: Evolution of magnetization dependent on time and gradient dephasing.*
- *Transition operator $\mathcal{T}$: Instantaneous RF pulse with flip angle α and phase Φ (i.e. a rotation of spins).*
- *Relaxation operator $\mathcal{E}$: Longitudinal and transversal relaxation with relaxation times T_1 and T_2, respectively.*
- *Isotropic diffusion operator $\mathcal{D}$: Signal attenuation due to diffusion effects dependent on time, diffusion and dephasing (constant gradients only, framed for the EPG from Ref. [11]).*

The exact representations of the operators published in literature are [1–3,8,11]:

$$\mathcal{S}(t_p \to t_{p+1}) = \mathcal{S}(k,\Delta k) : F_k \to F_{k+\Delta k}, \quad Z_k \to Z_k, \tag{7}$$

$$\mathcal{T}(t_p) = \mathcal{T}_\Phi(\alpha) = \begin{bmatrix} \cos^2\frac{\alpha}{2} & \exp(2i\Phi)\sin^2\frac{\alpha}{2} & -i\exp(i\Phi)\sin\alpha \\ \exp(-2i\Phi)\sin^2\frac{\alpha}{2} & \cos^2\frac{\alpha}{2} & i\exp(-i\Phi)\sin\alpha \\ -\frac{i}{2}\exp(-i\Phi)\sin\alpha & \frac{i}{2}\exp(i\Phi)\sin\alpha & \cos\alpha \end{bmatrix}, \tag{8}$$

$$\mathcal{E}(t_p \to t_{p+1}) = \mathcal{E}(\tau,T_1,T_2) = \begin{bmatrix} \exp\left(-\frac{\tau}{T_2}\right) & 0 & 0 \\ 0 & \exp\left(-\frac{\tau}{T_2}\right) & 0 \\ 0 & 0 & \exp\left(-\frac{\tau}{T_1}\right) \end{bmatrix}, \tag{9}$$

$$\mathcal{D}(t_p \to t_{p+1}) = \mathcal{D}(D,\tau,k,\Delta k) = \exp(-b_\tau \cdot D), \tag{10}$$

$$\text{with } b_\tau = \left(k + \frac{\Delta k}{2}\right)^2 \cdot \tau + \frac{\Delta k^2}{12} \cdot \tau. \tag{11}$$

All operators except for $\mathcal{T}$ are defined on a time interval $\tau = t_{p+1} - t_p$, while $\mathcal{T}$ acts instantly at the time points of the RF pulses. For operators that depend on k, a change of k to $k + \Delta k$ takes place for any given transversal state, while any given longitudinal state keeps its initial k.

The transition operator $\mathcal{T}$ does not depend on k. It realizes the same rotation for all states. In particular, $\mathcal{T}$ only mixes phase states of the same dephasing order of k [2]. Furthermore, the $\mathcal{T}$-operator acts on the total magnetization. In contrast, operators $\mathcal{S}$, $\mathcal{E}$ and $\mathcal{D}$ act on the difference between the actual and the equilibrium magnetization $\mathbf{M} - \mathbf{M}_0$. The latter is normalized to unity, $\mathbf{M}_0 = [0,0,1]^\dagger$.

The isotropic diffusion operator $\mathcal{D}$ acts differently on transversal and longitudinal phase states (see also below), since longitudinal states do not experience phase evolution, hence, the second term of Eq. (11) vanishes due to $\Delta k = 0$. Eqs. (10) and (11) were framed for the EPG calculus from Ref. [11]. It is to note that the relation is only defined for constant gradient g, i.e. $\Delta k = g\tau$. D is the scalar diffusion coefficient for isotropic diffusion.

Fig. 1 demonstrates a representative example for the use of the (1D) EPG framework as a repetition or introduction based on a multi-spin echo sequence with arbitrary flip angles and timing.

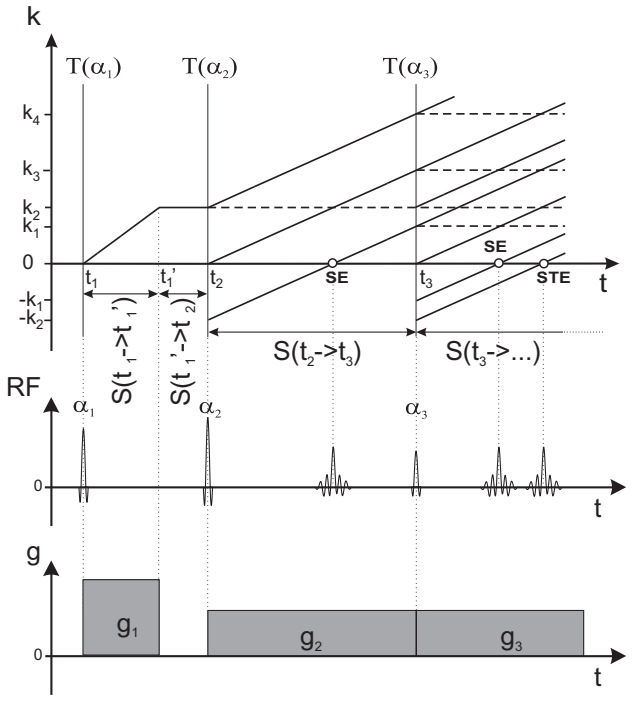

Fig. 1. Representative example for the use of the EPG. Note the direct relation between the EPG and the sequence diagram as shown. Continuous lines denote pathways of transversal *F*-states, dashed lines signify longitudinal *Z*-states. Only the salient $\mathcal{T}$- and $\mathcal{S}$-operators were noted, since only these show visible effects of splitting and evolving phase graphs. $\mathcal{E}$ and $\mathcal{D}$ merely influence the population of states. For reasons of simplicity, two rephasing pathways after the third RF pulse were excluded from the figure. They would lead to two further echoes at a later time.

Three different RF pulses (flip angles α_1, α_2, α_3) and three gradients with different durations and strengths g_1, g_2, g_3 were presumed.

Continuous lines represent transversal magnetization (*F*-states, Eqs. (2) and (3)) that evolve with time (*x*-axis). The slope of the transversal pathways directly corresponds to the active gradient strength, since k describes the dephasing of a given state and Δk is proportional to g (Eq. (1)). Hence, at locations where (ideally) no gradient exists, the *F*-states demonstrate horizontal lines, since no further dephasing takes place.

Dashed lines represent longitudinal magnetization (*Z*-states, Eq. (4)). These do not experience any phase evolution with time and are, thus, always horizontal lines. Generally, phase evolution such as dephasing and rephasing is depicted by changing k and accomplished by the shift operator $\mathcal{S}$, as indicated in the EPG diagram of Fig. 1.

Magnetization after an RF pulse can be regarded as a composition of three components, which was first described by Woessner [20]: (1) A transversal component that is unaffected by the RF pulse ('0°-pulse'). (2) Another transversal component that was refocused by an 180°-pulse. (3) A longitudinal component. This superposition of magnetization vectors is also known as the Woesssner decomposition [20]. In terms of the EPG this means that the $\mathcal{T}$-operator, representing RF pulses, splits any given EPG state with dephasing order k into three different new states: (1) A transversal state with identical k. (2) A transversal state with inverted k. (3) A longitudinal state with identical k. This behavior is directly reflected in the EPG diagram of Fig. 1, where each pathway splits into three new ones after the application of $\mathcal{T}$. The fractional populations of the new partition states, and therefore new pathways, depend on the applied flip angle and are described quantitatively by Eq. (8). Each of the three RF pulses also creates an additional FID represented by the transversal pathway starting from the *x*-axis in each case.

Besides the salient EPG operators $\mathcal{T}$ and $\mathcal{S}$, the relaxation operator $\mathcal{E}$ and the diffusion operator $\mathcal{D}$ act between the RF pulses and realize evolution of the spin system in terms of relaxation and diffusion effects. Both were not noted in Fig. 1 for a better overview.

Each transversal path that crosses the $k = 0$ line/*x*-axis characterizes the generation of an echo, i.e. an F_0-state meaning coherent magnetization exists. All echoes in Fig. 1 are denoted as circles and are labeled with their type of spin echo (SE) or stimulated echo (STE). This classification results from the source of the investigated pathway before the RF pulse: Either it was a transversal (SE) or longitudinal (STE) path before.

As a typical example, the vector of phase state constellations **F** directly after the third RF pulse in Fig. 1 can be calculated via the following sequence of matrix operations:

$$\begin{aligned}\mathbf{F}^{+}(t_3) = {} & \mathcal{T}(t_3)\mathcal{D}(t_2 \to t_3)\mathcal{E}(t_2 \to t_3)\mathcal{S}(t_2 \to t_3) \\ & \mathcal{T}(t_2)\mathcal{D}(t_1' \to t_2)\mathcal{E}(t_1' \to t_2) \\ & \mathcal{D}(t_1 \to t_1')\mathcal{E}(t_1 \to t_1')\mathcal{S}(t_1 \to t_1')\mathcal{T}(t_1)Z_0, \end{aligned} \tag{12}$$

where t_1, t_1', t_2, and t_3 denote the point of times when the respective operators start or end to act (see also operator list above). The superscript "+" denotes "directly after the pulse", which is a common notation in literature [8].

$\mathbf{F}^{+}(t_3)$ is the vector consisting of the phase state constellations generated through the sequence of matrix operators acting on the single initial Z_0-state, and, thus, describing the sequence. The Z_0 state contains the non-modulated longitudinal magnetization. It is therefore presumed that the MR sequence initially starts from the thermal equilibrium magnetization M_0, i.e. all *Z*-states and *F*-states vanish except for Z_0.

Eq. (12) has to be interpreted such that each operator acts on the present set of phase state constellations $\mathbf{F}(t_p)$ and creates a new one. The operators act successively or in the strict block-wise fashion as noted. In particular, occurring F_0-states represent generated echoes and their occupation equals to the corresponding echo amplitude. Fig. 1 displays an example for this effect, where an intermediate spin echo forms between the 2^{nd} and 3^{rd} RF pulse (black circle on the time axis).

$\mathbf{F}^{+}(t_3)$ has to contain nine transversal *F*-states and five longitudinal *Z*-states, as can be easily counted from the number of evolving pathways shown after the 3rd RF pulse in Fig. 1 (two transversal pathways at the bottom are not shown and one longitudinal pathway, arising from the Z_0-state, lies directly on the *x*-axis see figure caption).

2.2. Anisotropic diffusion regarded with the extended phase graph

The starting point to determine unrestricted anisotropic diffusion effects in the EPG is the Bloch–Torrey equation, which depicts the evolution of magnetization for diffusing spins in a liquid [12]. It is written here in the form used in Ref. [11]:

$$\frac{\partial \psi}{\partial t} = D_{\mathrm{mn}}\nabla_{\mathrm{m}}\nabla_{\mathrm{n}}\psi + i g_{\mathrm{m}} r_{\mathrm{m}} I_z \psi - \frac{1}{T_2} I_z^2 \psi - \frac{1}{T_1}(1 - I_z^2)\psi. \tag{13}$$

Here, ψ represents the difference of the magnetization density to the thermal equilibrium magnetization and varies in space and time: $\psi = \psi(\mathbf{r},t)$. **D** is the macroscopic effective self-diffusion tensor with the corresponding tensor elements $D_{\mathrm{mn}} = D_{\mathrm{nm}}$. $\mathbf{I}_z$ is the generator of rotation around the *z*-axis:

$$\mathbf{I}_z = \begin{bmatrix} 0 & +i & 0 \\ -i & 0 & 0 \\ 0 & 0 & 0 \end{bmatrix}, \quad \mathbf{I}_z^2 = \begin{bmatrix} 1 & 0 & 0 \\ 0 & 1 & 0 \\ 0 & 0 & 0 \end{bmatrix}. \tag{14}$$

For easier handling of the tensors and vectors an element-index description is used in Eq. (13) and in the following text. Any double occurring index implies a summation over this index over the whole range *x*, *y*, *z* ("Einstein notation").

Eq. (13) can be solved for unrestricted anisotropic diffusion by using the method of characteristics [21]. This mathematical solution is presented in Appendix A.1. Essentially the same solution is discussed in a more pictorial and intuitive way in the following text.

Unrestricted anisotropic diffusion motion in 3D position space is described by the diffusion propagator

$$P(\mathbf{r},t)=\frac{1}{\sqrt{|\mathbf{D}|(4\pi t)^3}}\exp\left(-\frac{\mathbf{r}^\dagger\mathbf{D}^{-1}\mathbf{r}}{4t}\right), \tag{15}$$

where $|\mathbf{D}|$ is the determinant and $\mathbf{D}^{-1}$ is the inverse of $\mathbf{D}$. Eq. (15) describes an "anisotropic Gaussian" broadening with time, its exponent representing a time dependent diffusion ellipsoid. In the limit as t tends to 0 the Gaussian tends to a delta peak. Eq. (15) is a solution of the Bloch–Torrey equation selected by the delta-functional initial condition.

Given an original magnetization distribution $\mathbf{M}(\mathbf{r},0)$ in position space at $t=0$, the evolution of magnetization due to diffusion after an elapsed time $\Delta t>0$ is given by the convolution:

$$\mathbf{M}(\mathbf{r},\Delta t)=P(\mathbf{r},\Delta t)*\mathbf{M}(\mathbf{r},0)=\int_V P(\mathbf{r}'-\mathbf{r},\Delta t)\cdot\mathbf{M}(\mathbf{r}',0)d^3r'. \tag{16}$$

According to the convolution theorem, Eq. (16) is equivalent to the product in the Fourier space representation:

$$\mathrm{FT}\{\mathbf{M}(\mathbf{r},\Delta t)\}=\mathrm{FT}\{P(\mathbf{r},\Delta t)\}\cdot\mathrm{FT}\{\mathbf{M}(\mathbf{r},0)\}, \tag{17}$$

$$\rightleftarrows\ \widetilde{\mathbf{M}}(\mathbf{k},\Delta t)=\widetilde{P}(\mathbf{k},\Delta t)\cdot\widetilde{\mathbf{M}}(\mathbf{k},0). \tag{18}$$

Here $\widetilde{\mathbf{M}}(\mathbf{k},\Delta t)$ represents diffusion affected magnetization in k-space. Reformulating it as a sum of transversal F-states and longitudinal Z-states directly leads to the EPG calculus represented by Eqs. (1)–(4). Then, $\widetilde{P}(\mathbf{k},\Delta t)$ directly signifies the EPG diffusion operator sought after.

Evaluating the Fourier transform of Eq. (15) leads to

$$\widetilde{P}(\mathbf{k},\Delta t)=\mathrm{FT}\left\{\frac{1}{\sqrt{|\mathbf{D}|(4\pi\Delta t)^3}}\exp\left(-\frac{\mathbf{r}^\dagger\mathbf{D}^{-1}\mathbf{r}}{4\Delta t}\right)\right\}, \tag{19}$$

$$=\exp\left(-\mathbf{k}^\dagger\mathbf{D}\mathbf{k}\Delta t\right)=\exp\left(-k_{\mathrm{m}}D_{mn}k_n\Delta t\right). \tag{20}$$

Eqs. (19) and (20) are only derived for a constant $\mathbf{k}$ within the time interval Δt so far. However, discretizing a given interval τ with changing $\mathbf{k}$ into many intervals Δt with different constant $\mathbf{k}$ and taking the limit $\Delta t\to 0$, yields the result for continuous $\mathbf{k}(t)$-values, i.e. k-space trajectories. Thus, the EPG operator for unrestricted anisotropic diffusion takes the following general form:

$$\mathcal{D}(\mathbf{k}(t),\tau)=\exp\left(-\int_{t=0}^{\tau}\mathbf{k}^\dagger(t)\mathbf{D}\mathbf{k}(t)dt\right)$$

$$=\exp\left(-\int_{t=0}^{\tau}k_{\mathrm{m}}(t)D_{mn}k_n(t)dt\right), \tag{21}$$

where $\mathbf{k}(t)$ denotes the k-space trajectory during the time interval τ. Eq. (21) emphasizes the fact that the exhibited diffusion weighting directly depends on the effective k-space trajectory.

In analogy to common literature where a b-matrix defines the level of total diffusion weighting a given NMR sequence exhibits [22,23], a 'b-matrix per time interval τ', $\mathbf{b}_\tau$ is defined in the following, which quantifies the exhibited diffusion weighting of an MR sequence in this time interval τ:

$$b_{\tau,\mathrm{mn}}(k_{\mathrm{m}}(t),k_{\mathrm{n}}(t),\tau)=\int_{t=0}^{\tau}k_{\mathrm{m}}(t)\cdot k_{\mathrm{n}}(t)dt. \tag{22}$$

Its definition in Eq. (22) (and its later use in Eq. (23), for instance) immediately shows that $\mathbf{b}_\tau$ has the direct characteristics of a tensor, thus, it will be referred to it in a more accurate way as the 'b-tensor per time interval τ' in the following text from now on.

For $m=n$, Eq. (22) leads to the calculation of the diagonal (principal axis) components of the effective b_τ-tensor, for $m\neq n$ the off-diagonal (cross) elements result.

With the introduction of the b_τ-tensor the derived diffusion operator $\mathcal{D}$ can be written in the simple form

$$\mathcal{D}(\mathbf{D},\mathbf{b}_\tau,\tau)=\exp\left(-\mathrm{Tr}(\mathbf{b}_\tau\mathbf{D})\right)=\exp\left(-b_{\tau,mn}D_{mn}\right). \tag{23}$$

Eqs. (21)–(23) determine the signal attenuation due to the diffusion motion of spins in a heterogeneous magnetic field for arbitrary $\mathbf{k}(t)$ in a time interval τ.

It is important to note that $\mathbf{b}_\tau$ is additive while tracing any given pathway in the EPG due to the block-wise definition of the EPG and its operators such as $\mathcal{D}$ in particular:

$$b_{\mathrm{mn}}^{(\mathrm{total})}=b_{\tau,\mathrm{mn}}^{(1)}+b_{\tau,\mathrm{mn}}^{(2)}+b_{\tau,\mathrm{mn}}^{(3)}+\cdots. \tag{24}$$

The superscript numbers in parentheses signifies the arbitrarily numbered sections of a given EPG. Relation (24) will be exploited for some of the exemplary calculations of $\mathcal{D}$ respective $\mathbf{b}_\tau$ in the "Validated Examples" section.

In the case of isotropic diffusion regarded in 1D-space, which is the most frequent approach found in literature, the integral of Eq. (22) reduces to

$$b_{\tau,1\mathrm{D}}(k(t),\tau)=\int_{t=0}^{\tau}k^2(t)dt. \tag{25}$$

Eq. (25) can be interpreted pictorially as a rotational solid around the time axis. Thus, the effective b_τ of an EPG coherence path under observation corresponds to the volume of its solid of revolution divided by π. This analogy is demonstrated in Fig. 2. A longitudinal and transversal state with a constant (background) gradient in a time interval τ are shown (no RF pulses). The different forms evolve due to the fact that for transversal states k changes linearly from $k^{(1)}$ to $k^{(2)}$ if a non-vanishing constant gradient is present (truncated cone/frustum). For longitudinal states k remains unchanged ($k=k^{(1)}$, cylinder).

In the following, the general anisotropic 3D diffusion operator $\mathcal{D}$ derived in Eq. (21) is solved for the most common application of transversal and longitudinal states simultaneously present with a rectangular (constant) gradient of arbitrary direction $\mathbf{g}$ during a time interval τ. For the solutions, it is important to evaluate the b_τ-integral from Eq. (22) for the different boundary conditions of F- and Z-states. Without loss of generality it is presumed that the spin system is initially described by the single dephasing coordinate $\mathbf{k}^{(1)}$. Then, a generic spin ensemble can be depicted by a linear superposition of such spin dephasing state, i.e. the vector of partition states.

Longitudinal Z-states. A Z-state does not experience phase evolution, although a non-vanishing gradient is present: $k_{\mathrm{m}}(t)=k_{\mathrm{m}}^{(1)}$. Thus, for a longitudinal state $\mathbf{b}_\tau$ defined in Eq. (22) takes the form

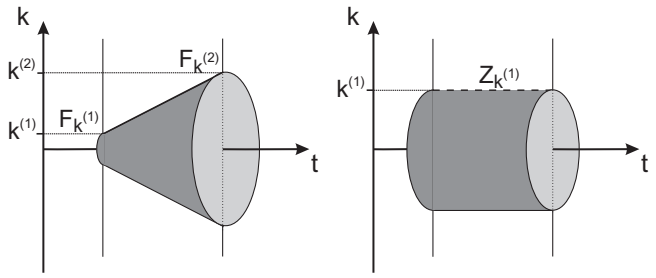

Fig. 2. Investigation of a typical F- and Z-state with a given initial dephasing $k^{(1)}$. The volume of the solid of revolution under the coherence path directly corresponds to the b_τ-factor for the regarded time interval τ (divided by π). Particularly, the solid of revolution represents a truncated cone for transversal F-states and a cylinder for longitudinal Z-states.

$$b^{\mathrm{L}}_{\tau,\mathrm{mn}}\left(k^{(1)}_{\mathrm{m}},k^{(1)}_{\mathrm{n}},\tau\right)=k^{(1)}_{\mathrm{m}}k^{(1)}_{\mathrm{n}}\tau. \tag{26}$$

Transversal F-states. For these states, $\mathbf{k}(t)$ increases linearly from a given $\mathbf{k}^{(1)}$ to $\mathbf{k}^{(2)}$ due to the constant gradient $\mathbf{g}$ within the time interval τ:

$$k_{\mathrm{m}}(t)=k^{(1)}_{\mathrm{m}}+\frac{k^{(2)}_{\mathrm{m}}-k^{(1)}_{\mathrm{m}}}{\tau}\cdot t. \tag{27}$$

Evaluating Eq. (22) for transversal states with Eq. (27) for two different components k_{m}, k_{n} leads to

$$b^{\mathrm{T}}_{\tau,\mathrm{mn}}\left(k^{(1)}_{\mathrm{m}},k^{(1)}_{\mathrm{n}},k^{(2)}_{\mathrm{m}},k^{(2)}_{\mathrm{n}},\tau\right) \tag{28}$$

$$=k^{(1)}_{\mathrm{m}}k^{(1)}_{\mathrm{n}}\tau+\frac{1}{2}k^{(1)}_{\mathrm{m}}\left(k^{(2)}_{\mathrm{n}}-k^{(1)}_{\mathrm{n}}\right)\tau+\frac{1}{2}k^{(1)}_{\mathrm{n}}\left(k^{(2)}_{\mathrm{m}}-k^{(1)}_{\mathrm{m}}\right)\tau +\frac{1}{3}\left(k^{(2)}_{\mathrm{m}}-k^{(1)}_{\mathrm{m}}\right)\left(k^{(2)}_{\mathrm{n}}-k^{(1)}_{\mathrm{n}}\right)\tau, \tag{29}$$

$$=b^{\mathrm{L}}_{\tau,\mathrm{mn}}\left(k^{(1)}_{\mathrm{m}},k^{(1)}_{\mathrm{n}},\tau\right)+\frac{1}{2}k^{(1)}_{\mathrm{m}}\left(k^{(2)}_{\mathrm{n}}-k^{(1)}_{\mathrm{n}}\right)\tau +\frac{1}{2}k^{(1)}_{\mathrm{n}}\left(k^{(2)}_{\mathrm{m}}-k^{(1)}_{\mathrm{m}}\right)\tau+\frac{1}{3}\left(k^{(2)}_{\mathrm{m}}-k^{(1)}_{\mathrm{m}}\right)\left(k^{(2)}_{\mathrm{n}}-k^{(1)}_{\mathrm{n}}\right)\tau. \tag{30}$$

Eqs. (29) and (30) show that the transversal b_τ-tensor is composed of two components: The first term corresponds to the longitudinal b^{L}_τ-tensor and would be the exact solution if $\mathbf{k}$ was not changing, the other three terms arise due to the present gradient that leads to further dephasing and, thus, further signal attenuation.

Finally, since $\mathbf{b}_\tau$ has a different form for *F*- and *Z*-states and depends on $\mathbf{k}$, it is convenient to describe the diffusion attenuation as the action of the following diffusion operator:

$$\mathcal{D}=\begin{bmatrix}\mathcal{D}^{\mathrm{T}} & 0 & 0\\ 0 & \mathcal{D}^{\mathrm{T}} & 0\\ 0 & 0 & \mathcal{D}^{\mathrm{L}}\end{bmatrix}, \tag{31}$$

where

$$\mathcal{D}^{\mathrm{L}}=\exp\left(-b^{\mathrm{L}}_{\tau,mn}D_{mn}\right)=\exp\left(-\mathrm{Tr}\left(\mathbf{b}^{\mathbf{L}}_{\tau}\mathbf{D}\right)\right), \tag{32}$$

$$\mathcal{D}^{\mathrm{T}}=\exp\left(-b^{\mathrm{T}}_{\tau,mn}D_{mn}\right)=\exp\left(-\mathrm{Tr}\left(\mathbf{b}^{\mathbf{T}}_{\tau}\mathbf{D}\right)\right). \tag{33}$$

3. Calculation of representative examples

In the following, a few examples will be given to further validate the calculated results, repeat the usage of the EPG, and to demonstrate its great potential for the calculation of diffusion effects.

3.1. Published solution for isotropic diffusion in 1D

There is a known solution for the signal attenuation due to isotropic diffusion while a piece-wise constant gradient is present [11], which is a special case of the presently considered case. Framed for the EPG calculus this solution takes the form

$$\mathcal{D}_{1\mathrm{D}}=\exp\left(-\left(k+\frac{\Delta k}{2}\right)^2\cdot\tau\cdot D\right)\cdot\exp\left(-\frac{\Delta k^2}{12}\cdot\tau\cdot D\right). \tag{34}$$

Here, D is the isotropic diffusion coefficient and k is the magnitude of the wave vector in the constant direction of the applied gradient g. Δk is the change of k due to g in the investigated interval τ, being $\Delta k = g\tau$. Eq. (34) represents the compact form of Eqs. (10) and (11) used in the EPG operator overview in the Introduction section.

Simplifying the derived longitudinal and transversal 3D diffusion operators of Eqs. (32) and (33) to 1D in the same way leads to:

$$\mathcal{D}^{\mathrm{L}}_{\text{iso-1D}}=\exp\left(-b^{\mathrm{L}}_{\tau}D\right), \tag{35}$$

$$\text{with } b^{\mathrm{L}}_{\tau}=\left(k^{(1)}\right)^2\tau, \tag{36}$$

$$\mathcal{D}^{\mathrm{T}}_{\text{iso-1D}}=\exp\left(-b^{\mathrm{T}}_{\tau}D\right), \tag{37}$$

$$\text{with } b^{\mathrm{T}}_{\tau}=\left(k^{(1)}\right)^2\tau+\left(k^{(2)}-k^{(1)}\right)\left(2k^{(1)}+k^{(2)}\right)\frac{\tau}{3}, \tag{38}$$

$$\text{or } b^{\mathrm{T}}_{\tau}=\left(k^{(1)}+k^{(2)}\right)^2\frac{\tau}{4}+\left(k^{(1)}-k^{(2)}\right)^2\frac{\tau}{12}. \tag{39}$$

Hereby the already described b_τ-tensor in 1D (scalar b_τ, Eq. (25)) was solved for *F*- and *Z*-states in an equivalent way as was done for the 3D anisotropic representation (Eqs. (26)–(30)).

Considering that for constant g by definition is $k+\Delta k/2 = (k^{(1)}+k^{(2)})/2$ and $(k^{(1)}-k^{(2)})^2=\Delta k^2$ directly proves that Eqs. (34) and (37) with (39) are equivalent. Thus, the operators coincide for transversal states. For longitudinal states, setting $\Delta k = 0$ and considering that $k = k^{(1)}$ directly shows that the diffusion operators for longitudinal states coincide as well (Eqs. (34) and (35) with (36)).

Note that any operators $\mathcal{A}$ defined in Ref. [11] take the form $U\mathcal{A}U^{-1}$ in the present notations, where the matrix U is defined by the linear transformation (2)–(4).

3.2. Simple pulsed gradient spin echo sequence

Consider a typical pulsed gradient spin echo sequence (PGSE or Stejskal–Tanner sequence [24]) as shown in Fig. 3: Two monopolar, rectangular gradients each of duration δ, both with the same direction and strength g and a mutual time distance of Δ. The whole MR sequence is regarded as six different sections: 90°-excitation pulse, first gradient g of duration δ, dead time τ_{d}, 180°-refocusing pulse, dead time τ_{d}, second gradient g of duration δ, and finally the spin echo. The black circle in the EPG signifies this spin echo formation at echo time *TE*. Relaxation is neglected ($\mathcal{E}\equiv 1$), yet, can be included very easily if desired.

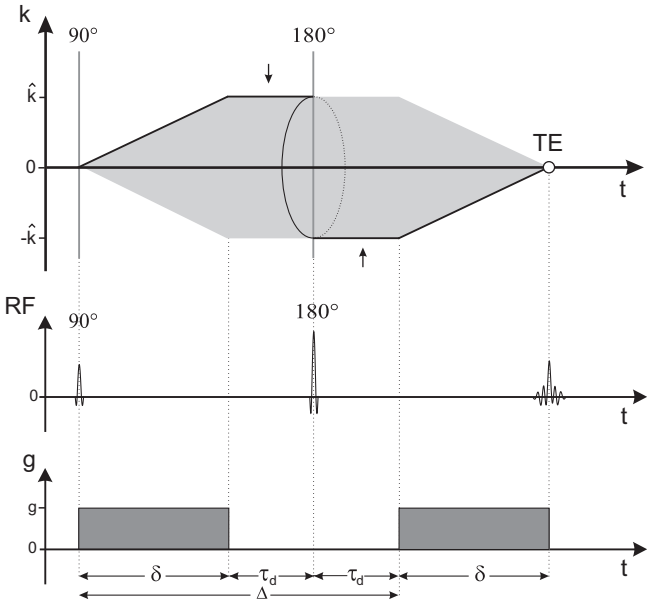

Fig. 3. EPG and sequence diagram for the simple PGSE sequence. In time intervals with (ideally) no gradient present transversal states also demonstrate horizontal phase graphs in the diagrams (two black arrows). The light gray shaded area between the phase graphs represents the corresponding solid of revolution, its volume being proportional to the resulting *b*-factor. Note that both dead times τ_{d} substantially contribute to the diffusion weighting as can be seen from the rotational solid.

The echo intensity at *TE* is determined by the following matrix operations describing the PGSE in terms of the EPG calculus:

$$\begin{aligned}\mathbf{F}_{\mathrm{PGSE}}(TE) = {} & \mathcal{D}(\delta+2\tau_\mathrm{d}\to 2\delta+2\tau_\mathrm{d})\mathcal{S}(\delta+2\tau_\mathrm{d}\to 2\delta+2\tau_\mathrm{d})\\ & \mathcal{D}(\delta+\tau_\mathrm{d}\to \delta+2\tau_\mathrm{d})\mathcal{T}(\delta+\tau_\mathrm{d})\mathcal{D}(\delta\to\delta+\tau_\mathrm{d})\\ & \mathcal{D}(0\to\delta)\mathcal{S}(0\to\delta)\mathcal{T}(t=0)Z_0. \end{aligned} \tag{40}$$

For brevity, the operators are noted as being dependent on the time when they start and end to act, similar to the way in Eq. (12) near the beginning of the text. The notation used is in close agreement with Ref. [24].

Though Eq. (40) may seem complicated or lengthy, it has to be considered that this is still a quite general representation, since the flip angles and gradients are not defined in the equation, yet. For example, the first pulse is an ideal excitation pulse, thus, all magnetization will be excited into the F_0-state: $\mathcal{T}_{90^\circ}(90^\circ)Z_0 \to F_0 = 1$. $\mathcal{T}$ is also very simple for 180°-refocusing pulses.

As can be deduced from the EPG and the pulse sequence, only one transversal path to trace exists, which forms the later echo. No branching of pathways due to imperfect refocusing occurs. Hence, no longitudinal pathways participate in signal formation. This observation can be directly exploited to use an even faster way to determine the total *b*-factor of the PGSE sequence, and thus its diffusion weighting. Due to the block-wise definition of the EPG all four piece-wise b_τ along the given pathway add up (Eq. (24)):

$$b_{\mathrm{PGSE}} = b_\tau^{(1)} + b_\tau^{(2)} + b_\tau^{(3)} + b_\tau^{(4)}. \tag{41}$$

However, this faster solution will not be pursued further. Instead, the operators and the vector of states **F** will be explicitly defined in a very extensive way to demonstrate and repeat the usage of the EPG including diffusion effects.

It is $\mathcal{T}(\delta+\tau_\mathrm{d}) = \mathcal{T}_{0^\circ}(180^\circ)$ and $Z_0 = 1$, since the magnetization is initially in the thermal equilibrium. Presuming that both gradients cause the same shift of $\Delta k = \hat{k}$ leads to the shift operations $\mathcal{S}(0\to\delta) = \mathcal{S}(\delta+2\tau_\mathrm{d}\to 2\delta+2\tau_\mathrm{d}) = \mathcal{S}(k,\hat{k}) : F_k \to F_{k+\hat{k}}$.

For the definition of the (1D) diffusion operators different representations are available from the first example. Since Δk was already defined, the most practical form is the compact $k-\Delta k$–representation from Eq. (34) or Eqs. (10) and (11). Then, the diffusion operators correspond to $\mathcal{D}(0\to\delta) = \mathcal{D}(D,\delta,k,\hat{k}) = \mathcal{D}(\delta+2\tau_\mathrm{d}\to 2\delta+2\tau_\mathrm{d})$ and $\mathcal{D}(\delta\to\delta+\tau_\mathrm{d}) = \mathcal{D}(D,\tau_\mathrm{d},k,0) = \mathcal{D}(\delta+\tau_\mathrm{d}\to\delta+2\tau_\mathrm{d})$. For the latter two operators was taken into account that all gradients vanish, i.e. $g = 0$, and therefore is $\Delta k = 0$. It can be already seen that the symmetry of the sequence around the refocusing pulse is directly reflected in the mutual identity of operators. *k* is still undefined such that it depends on the state the operators act on.

Assembling the sections in a very detailed manner leads to:

$$\text{Section 1 at } t=0 : F_0^+ = \mathcal{T}_{90^\circ}(90^\circ)Z_0^- \tag{42}$$

$$\text{Section 2} \equiv [0;\delta] : F_{\hat{k}}^+ = \mathcal{D}(D,\delta,0,\hat{k})\mathcal{S}(0,\hat{k})F_0^- \tag{43}$$

$$\text{Section 3} \equiv [\delta;\delta+\tau_\mathrm{d}] : F_{\hat{k}}^+ = \mathcal{D}(D,\tau_\mathrm{d},\hat{k},0)F_{\hat{k}}^- \tag{44}$$

$$\text{Section 4 at } t=\delta+\tau_\mathrm{d} : \begin{bmatrix}0\\F_{-\hat{k}}\\0\end{bmatrix}^+ = \mathcal{T}_{0^\circ}(180^\circ)\begin{bmatrix}F_{\hat{k}}\\0\\0\end{bmatrix}^- \tag{45}$$

$$\text{Section 5} \equiv [\delta+\tau_\mathrm{d};\delta+2\tau_\mathrm{d}] : \begin{bmatrix}0\\F_{-\hat{k}}\\0\end{bmatrix}^+ = \mathcal{D}(D,\tau_\mathrm{d},-\hat{k},0)\begin{bmatrix}0\\F_{-\hat{k}}\\0\end{bmatrix}^- \tag{46}$$

$$\begin{aligned}\text{Section 6} \equiv [\delta+2\tau_\mathrm{d};2\delta+2\tau_\mathrm{d}] : & \begin{bmatrix}0\\F_0\\0\end{bmatrix}^+\\ = {} & \mathcal{D}(D,\delta,-\hat{k},\hat{k})\mathcal{S}(-\hat{k},\hat{k})\begin{bmatrix}0\\F_{-\hat{k}}\\0\end{bmatrix}^- \end{aligned} \tag{47}$$

Here, the superscripts "+" and "−" were generalized to mean a vector of EPG states before ("−") and after ("+") the application of the operators in the investigated section. The 180°-pulse inverts $\hat{k}$ and exchanges the populations of the dephasing $F_{\hat{k}}$- and the rephasing $F_{-\hat{k}}$-state (refocusing behavior), as can be also seen by the matrix representation of the $\mathcal{T}$ operator in Eq. (8).

The result vector of EPG states in Eq. (47) directly reflects the observation from Fig. 3 that only a completely rephased F_0-state, i.e. an echo, is present at the time *TE*. It is a pure spin echo.

In this example, dephasing is quantified in units of $\hat{k} = g\delta$.

The complete chain for quantifying the echo intensity, which is the occupation of state $F_0(TE)$, then equals to:

$$\begin{aligned}F_0(TE) = {} & \exp\left(-\frac{\hat{k}^2}{4}\delta D\right)\exp\left(-\frac{\hat{k}^2}{12}\delta D\right)\\ & \cdot\exp\left(-\hat{k}^2\tau_\mathrm{d}D\right)\cdot\exp\left(-\hat{k}^2\tau_\mathrm{d}D\right)\\ & \cdot\exp\left(-\frac{\hat{k}^2}{4}\delta D\right)\exp\left(-\frac{\hat{k}^2}{12}\delta D\right) \end{aligned} \tag{48}$$

$$= \exp\left(-\frac{2}{3}\hat{k}^2\delta D\right)\exp\left(-2\hat{k}^2\tau_\mathrm{d}D\right). \tag{49}$$

With a little previous practice the result of Eq. (49) could have been directly written out without 'the detour' via Eqs. (42)–(47).

Though both dead times do not display any phase evolution ($\Delta k = 0$), there is, indeed, effective diffusion weighting due to the presence of dephased magnetization (previous phase history: $k \neq 0$, Fig. 3).

Considering the relations $k = g\delta$ from Eq. (1) and $2\tau_\mathrm{d} = \Delta - \delta$, Eq. (49) is equivalent to stating that the total *b*-factor for the PGSE sequence is

$$b_{\mathrm{PGSE}} = g^2\delta^2\cdot\left(\Delta-\frac{\delta}{3}\right). \tag{50}$$

This result is identical to the well-known solution from Stejskal and Tanner [24].

3.3. Simple pulsed gradient stimulated echo sequence

Applying the framework in a similar way to the problem of a pulsed gradient stimulated echo sequence [25], leads to identical results for the weighting terms with the findings of Woessner [20] and Tanner [25]. To prove this is left as an exercise to the reader.

3.4. Diffusion sensitivity of a RARE sequence with low constant flip angles

The presented framework, i.e. the EPG with diffusion effects, is applied to a contemporary RARE (TSE, FSE) sequence with a user-defined constant flip angle α [1,17]. As previous works about and with the EPG already showed, a 1D dephasing coordinate is often sufficient for understanding the generic response of multi-pulse sequences such as RARE [2,26,27], which usually is the read-gradient direction. The same is done for the next two examples to keep this manuscript within a reasonable scope.

Fig. 4 shows the sequence diagram of such a RARE sequence. Idealized rectangular gradient shapes were presumed, because the difference in the results compared to simulating realistic trapezoidal gradient shapes is negligible (unpublished work) and, moreover, it does not lead to much further insight. However, it would be fairly easy to implement.

The following given scenario using realistic protocol parameters for a RARE sequence is presumed: field of view (FOV) = 220 mm, matrix = 256, echo time (TE) = 80 ms, echo spacing (ESP) = 8.0 ms,

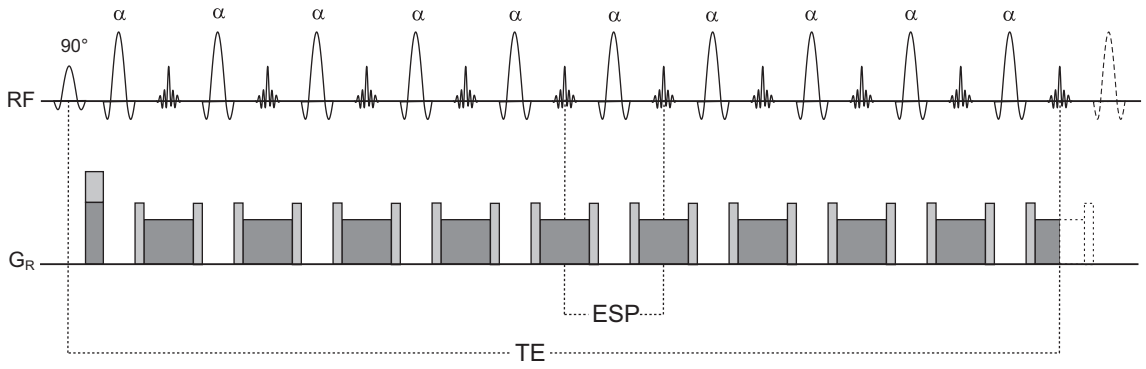

Fig. 4. Sequence diagram depicting a RARE sequence with the read-gradient direction as the one-dimensional dephasing coordinate, being the direction with the strongest gradients. After the 90° excitation pulse refocusing pulses with an arbitrary constant flip angle α follow. Additional gradient spoilers were considered. The sketch is true to scale.

echo train length (ETL) = 11 or greater, bandwidth = 264 Hz/px, the durations of the excitation and refocusing RF pulses are 2.56 ms each. This will result in the following approximate gradient pulse settings: combined read dephase and spoiler gradient in the 1st interval $G_{R\text{-}Sp\text{-}1} = 15.0$ mT/m, $\tau_{R\text{-}Sp\text{-}1} = 1.44$ ms; read encoding gradient 2nd and following intervals $G_{R\text{-}2} = 7.2$ mT/m, $\tau_{R\text{-}2} = 4.0$ ms; pair of read spoilers with $G_{Sp\text{-}2} = 9.9$ mT/m, $\tau_{Sp\text{-}2} = 0.72$ ms each. The sketch in Fig. 4 is true to scale for the gradient amplitudes and the whole sequence timing.

The necessary EPG operators $\mathcal{S}$, $\mathcal{T}$, $\mathcal{E}$, $\mathcal{D}$ were defined in accordance with the chosen protocol parameters, based on their definition in the operator list of Eqs. (7)–(11). For a quick and comfortable investigation of the example, the EPG concept with its operators was translated into a MATLAB script (The Mathworks, Natick, MA, USA). Since the EPG is based on calculations with matrices and vectors, it is a task well suited for computers and fairly easy to program (see also Appendix A).

In the following, a virtual tissue with realistic relaxation times of $T_1 = 1000$ ms and $T_2 = 100$ ms as well as a diffusion coefficient of $D = 0.001$ mm^2/s is introduced for simulations.

Fig. 5, left side, displays the resulting signal response depending on the refocusing flip angle α. The extreme cases are $\alpha = 0°$ and $\alpha = 180°$ representing the cases of no refocusing and a standard RARE with perfect refocusing, respectively. The signal curve is clearly dominated by the maximal achievable signal intensity for a RARE sequence in dependence of α. Its shape is a $\sin(\alpha/2)$-function [28].

Fig. 5, right side, shows the net b-factor to expect in dependence of the constant flip angle α. As can be seen, the diffusion sensitivity

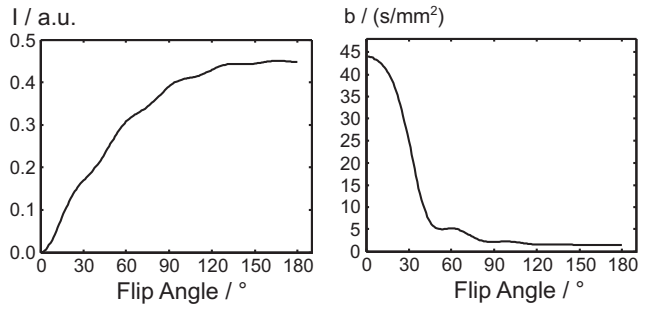

Fig. 5. Left: Simulated signal response measured with a RARE sequence depending on the flip angle α, explicitly considering relaxation and diffusion effects. The signal curve is clearly dominated by the general signal behavior of a RARE sequence. Right: Dependence of the total b-factor on the flip angle α. For RARE sequences with high flip angles the diffusion weighting is negligible. For low flip angles, however, b becomes more pronounced.

of a RARE sequence is practically negligible even for moderate refocusing flip angles. Interestingly, the b-factor considerably increases for quite low flip angles. This effect can be explained by the fact that for such low flip angles a great fraction of the magnetization is either well dephased transversal or 'stored' longitudinal magnetization. Both types experience noticeable diffusion weighting (see Section 2).

In terms of the EPG, low α mean the occupation of F- and Z-partition states of high order k. Since the signal attenuation due to diffusion is proportional to k^2, the diffusion sensitivity of a RARE sequence with low refocusing flip angle α has to increase considerably and therefore b as well.

3.5. Diffusion sensitivity of a RARE sequence with variable flip angles

As a variant from the last example to further show the considerable potential of the EPG approach with diffusion effects, the concept is applied to a modern RARE with variable refocusing flip angles, using the TRAPS principle [29].

The same RARE sequence with identical protocol parameters as in the last section is used except for the flip angles and that ETL is at least 14. The new course of variable flip angles is outlined in Fig. 6, left side, and was taken from Ref. [30]: Initial preparation pulses down to 60° followed by an ascending linear ramp of refocusing flip angles back to 180° are analyzed.

The given task can be easily solved with the already developed tools: Since the developed EPG concept allows for arbitrary flip angles, the mentioned MATLAB code or any other software implementation has only to be adapted to the fact that α changes with the RF pulse number and that a longer ETL is investigated.

Fig. 6, left side, shows the refocusing flip angle schedule presumed for the RARE experiment. It represents a realistic TRAPS-RARE experiment [29,30]. The net b-factor b_{tot} depending on the echo number is displayed in the center. Naturally, b_{tot} increases with the number of echoes due to the accumulating diffusion effect. However, the effective b-factor per echo interval $b_{\tau-eff}$ is very different from interval to interval as is explicitly shown in Fig. 6, right side. The main reason definitely being the significant variation of flip angles that leads to pronounced changes in the occupation of partition states in the EPG representation.

At this point, it is refrained from further discussing the given examples since the presented results and effects are inherent to the investigated types of (more complex) sequences; they are not inherent to the EPG framework itself. Thus, a proper analysis including a detailed discussion is beyond the scope of this work. However, they may be adequate to indicate the potential of the EPG framework with diffusion effects.

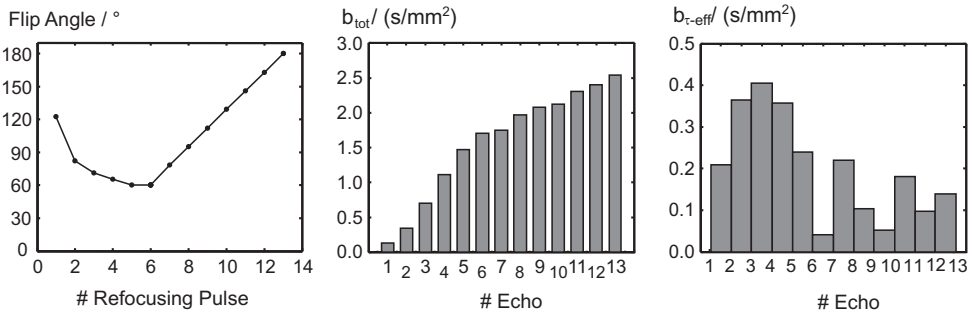

Fig. 6. Diffusion sensitivity of a RARE experiment with variable flip angles using TRAPS. Left: Course of refocusing flip angles depending on the RF pulse number. The discrete data points were connected for improved visibility. Center: Total *b*-factor the RARE sequence exhibits until the given echo number from 1 to 13. Right: Partial effective *b*-factor for each echo spacing, i.e. between the different echoes. The contributions to the total *b*-factor b_{tot} vary considerably.

4. Discussion

Diffusion effects and diffusion weighted imaging (DWI) have been extensively used in biomedical imaging [15,20,24,25,31,32]. DWI is usually achieved by a preparation scheme based on the fairly simple PGSE sequence [24] or, less frequently, based on stimulated echo schemes [25]. Mathematical solutions to characterize the effective diffusion weighting of these preparation schemes exist [20,24,25,31] since the early age of MR.

In 'diffusion-less' MR imaging fast imaging sequences with arbitrary refocusing flip angles have gained interest especially for high-field MR, where the use of 180° flip angles is limited by SAR, and constant and homogeneous flip angles can not be maintained due to B_1 inhomogeneities [14,26–30,33–38].

Modified RARE(TSE, FSE)-sequences have always sustained and in recent times even regained some interest as read-out modules in DWI [39–41], since they are less sensitive to field inhomogeneity effects compared to echo planar imaging (EPI) sequences, the standard read-out type. However, describing the signal response or calculating the effective *b*-tensors of such advanced sequences for DWI or diffusion tensor imaging (DTI, [22,23]) is considerably more complex. Up to date, existing solutions are either numerically based and/or very tedious for even moderately complex sequences [20,42]. Some of the better known solutions are limited to 180° RF pulses only [43,44], isotropic diffusion, constant gradients, single gradient directions [11]. These disadvantages aggravate substantially if RF pulses with low flip angles and gradients with multiple and arbitrary gradient shapes are employed.

The EPG calculus is a means to depict the magnetization response of MR sequences in an efficient and intuitive way even for large numbers of RF pulses and arbitrary gradients [1–3,8]. In this work, it was demonstrated that the EPG calculus affords a visualization of the mathematically exact solution to the Bloch–Torrey equation using the method of characteristics. A new operator $\mathcal{D}$ for the EPG calculus (Eq. (21)) was introduced which accounts for anisotropic diffusion effects on the signal attenuation. This allows for determining the accurate signal response of complex pulse sequences including diffusion effects by only a few simple matrix operations, i.e. a sequence of operators acting on dephasing (partition) states. This results in a high computational efficiency, but also permits the pictorial and intuitive understanding of echo formation within the framework of the EPG. Thus, novel diffusion experiments such as Hyperecho-diffusion [34,45,46] or double wave vector diffusion [47] may now be characterized in the compact block-wise, successive description of the EPG.

Since Eqs. (21) and (22) represent an exact solution even for arbitrary gradient time courses with arbitrary variable directions, it is fairly easy to account for their precise effect on diffusion quantifications by evaluating the corresponding integrals and, thus, defining the appropriate anisotropic diffusion operators. This ensures that the theoretical depiction of MR diffusion experiments reflects the real time course of the gradients, rather than a sequence of idealized rectangular gradient shapes.

Current limitations of the EPG based approach are that RF pulses are regarded as instantaneous. This hard-pulse approximation is also used in the standard description of diffusion imaging and is valid as long as diffusion displacements during the pulse are small. In principle, shaped soft pulses could be incorporated into the EPG description by using a DANTE approach, in which arbitrarily shaped RF pulses are decomposed into a sequence of instantaneous RF pulses with low flip angle [11,48,49]. More realistic effects like restricted diffusion could be also considered by use of a more general description of diffusion in terms of effective medium [50] or the consideration of other diffusion models.

Conventional phase graph approaches such as the partition state algorithm require to trace all existing pathways to determine the echo intensity [20,42]. Since the number of signal formation pathways grows with the number N of refocusing pulses by a factor of 3^{N-1}, this approach becomes unfeasible for even a modest number of refocusing pathways. By using the EPG calculus a single quantitative value k serves to depict the previous phase histories at the beginning of an investigated sequence section. The complexity of calculating effective diffusion weighting, thus, only grows linearly with N.

In literature, it is common to use integral values of k as a mere label for the phase state constellations $(F_{\pm 1}, Z_1, F_{\pm 2}, \ldots)$, for instance. This simplification is valid to describe mechanisms that do not depend on the absolute dephasing k (1D) or $\mathbf{k}$ (3D). This applies to the operators used for dephasing ($\mathcal{S}$), RF pulses ($\mathcal{T}$), and relaxation ($\mathcal{E}$).

In order to incorporate diffusion the actual k-space trajectory $\mathbf{k}(t)$ has to be considered (Eq. (21)), since diffusion dependent signal attenuation depends on $\mathbf{k}$ and all calculations have to be performed with the exact $\mathbf{k}$ values. Particularly, it should be noted that diffusion dependent signal attenuation increases quadratically with $|\mathbf{k}|$ (see also Figs. 2 and 3). Higher dephasing states therefore show much stronger diffusion effects than states of low dephasing.

The examples presented in this work served for the validation of the algorithm and to demonstrate the mechanism of how calculations of diffusion effects within the framework of the EPG concept are performed. Results for the RARE (TSE, FSE)-sequences illustrate the potential of our approach.

Future studies will include the study of advanced MR diffusion techniques such as q-space imaging [51], diffusion spectroscopic imaging (DSI) [52], or high-angular-resolution diffusion imaging (HARDI) [53], as well as diffusion weighting by Hyperecho and TRAPS sequences [29,34,45,46].

5. Conclusion

An anisotropic diffusion operator for the EPG calculus was introduced that allows for an easy, fast and exact calculation of *b*-tensors and diffusion dependent signal attenuations for multi-pulse MR sequences with arbitrary flip angles, phases, and gradients. Although not specifically considered in the Examples section, the developed algorithm can be easily extended to include the derived anisotropic diffusion operator. The use of the EPG calculus enables a high efficiency for the quantitation of echo intensities and can be easily implemented using common programming tools like MATLAB or C++.

Appendix A

A.1. Possible availability of source code

Interested readers may obtain a framework of programming source code from the authors for simulating extended phase graphs. This software framework, called 'EPGspace', was also used for the presented examples and, thus, includes the assessment of diffusion effects. Please contact the first and corresponding author (MW) for further information.

A.2. Solution of the Bloch–Torrey equation for anisotropic diffusion using the method of characteristics

Here, a solution of the Bloch–Torrey equation (Eq. (13)) formulated in conventional mathematical terms is presented. It is convenient to begin with a substitution that accounts for relaxation:

$$\psi = \exp\left(-I_z^2 \cdot t/T_2 - (1 - I_z^2) \cdot t/T_1\right)\chi. \tag{A.1}$$

The simplest way to work with the exponent of the matrix shown in Eq. (A.1) is to expand the magnetization vector χ in the eigenvectors and to replace the matrix with the corresponding eigenvalues. In practice this means that matrix I_z^2 is one or zero when acting on the transverse or longitudinal components of χ, respectively (Eq. (14)). Matrix $(1 - I_z^2)$ gives zero or unity correspondingly. The residual equation for χ takes the form

$$\frac{\partial\chi}{\partial t} = D_{mn}\nabla_m\nabla_n\chi + ig_m r_m\chi. \tag{A.2}$$

For clarity, this equation is first solved in one spatial dimension. A generalization for the anisotropic diffusion in three dimensions is presented at the end of this appendix.

In one spatial dimension Eq. (A.2) takes the form

$$\frac{\partial\chi}{\partial t} = D\frac{\partial^2\chi}{\partial r^2} + ig(t)r\chi. \tag{A.3}$$

This equation becomes simpler when formulated for the Fourier transformed magnetization $\tilde{\chi}(k)$

$$\frac{\partial\tilde{\chi}}{\partial t} + g(t)\frac{\partial\tilde{\chi}}{\partial k} = -Dk^2\tilde{\chi}. \tag{A.4}$$

This equation is a particular case of the following equation, which is now considered in order to make the idea of the solution more apparent:

$$a(t,k,\tilde{\chi})\frac{\partial\tilde{\chi}}{\partial t} + b(t,k,\tilde{\chi})\frac{\partial\tilde{\chi}}{\partial k}\tilde{\chi} = c(t,k,\tilde{\chi}). \tag{A.5}$$

For simplicity, $\tilde{\chi}$ is temporarily considered as a scalar variable rather than the magnetization vector. In this case, any solution to Eq. (A.5) describes a surface $\tilde{\chi}(t,k)$. The coefficients *a*, *b* and *c* can be considered as the three components of a vector, **v**, which is defined in each point of three-dimensional space of variables *t*, *k* and $\tilde{\chi}$. In terms of these quantities, Eq. (A.5) is a statement that vector **v** is tangential to the surface at each point. To show this, one needs first to write the differential of $d\tilde{\chi}$ on the surface and represent it in the form of a scalar product of two vectors:

$$\left(\frac{\partial\tilde{\chi}}{\partial t}, \frac{\partial\tilde{\chi}}{\partial k}, -1\right)(dt, dk, d\tilde{\chi})^\dagger = 0. \tag{A.6}$$

This reveals the fact that the first vector, denoted for brevity as **n**, is normal to the surface. Eq. (A.5) can now be written as **nv** = 0, which proves the above statement.

The vector field **v** defines lines to which this vector is tangential at each points, the so-called integral curves. The plane $\tilde{\chi}(t,k)$ can be considered as the union of all such curves that are selected by the initial condition at $t = t_0$. Along the integral curve, the differential of the position is parallel to vector **v**:

$$dt = a(t,k,\tilde{\chi})du, \tag{A.7}$$

$$dk = b(t,k,\tilde{\chi})du, \tag{A.8}$$

$$d\tilde{\chi} = c(t,k,\tilde{\chi})du, \tag{A.9}$$

where *u* is a parameter along the curve. This system of equations can be solved using the explicit form of *a*, *b* and *c*. The first equation gives $u = t - t_0$. The second and the third equation yield the solution

$$k(t) = k(t_0) + \int_{t_0}^{t} g(t')dt', \tag{A.10}$$

$$\tilde{\chi}(t) = \tilde{\chi}(t_0)\mathrm{e}^{-D\int_{t_0}^{t} k(t')^2 dt'}. \tag{A.11}$$

In the context of EPGs, the magnetization in *k*-space is a sum of delta-functional contributions, the spins. In this case the equations above describe the evolution of the wave vector and of the corresponding magnitude, respectively.

The generalization to the general case of three-dimensional magnetization is straightforward. One has to apply the above logic to each of three equations for individual components of the magnetization treated in five-dimensional space. This leads to equivalent expressions for the definition of k_m (Eq. (1)) and the resulting solution for the anisotropic diffusion operator $\mathcal{D}$ (Eq. (21)).

References

[1] J. Hennig, Multiecho imaging sequences with low refocusing flip angles, J. Magn. Reson. 78 (1988) 397–407.
[2] J. Hennig, Echoes—how to generate, recognize, use or avoid them in MR-imaging sequences. Part I, Conc. Magn. Reson. 3 (1991) 125–143.
[3] J. Hennig, Echoes—how to generate, recognize, use or avoid them in MR-imaging sequences. Part II, Conc. Magn. Reson. 3 (1991) 179–192.
[4] P. Mansfield, P.K. Grannell, "Diffraction" and microscopy in solids and liquids by NMR, Phys. Rev. 12 (1975) 3618–3634.
[5] P. Mansfield, Multi-planar image formation using NMR spin echoes, J. Phys. C 10 (1977) L55–L58.
[6] S. Ljunggren, A simple graphical representation of fourier-based imaging methods, J. Magn. Reson. 54 (1983) 338–343.
[7] F. Bloch, Nuclear induction, Phys. Rev. 70 (1946) 460–474.
[8] K. Scheffler, A pictorial description of steady-states in rapid magnetic resonance imaging, Conc. Magn. Reson. 11 (1999) 291–304.
[9] N.N. Lukzen, A.A. Savelov, Analytical derivation of multiple spin echo amplitudes with arbitrary refocusing angle, J. Magn. Reson. 185 (2007) 71–76.
[10] N.N. Lukzen, M.V. Petrova, I.V. Koptyug, A.A. Savelov, R.Z. Sagdeev, The generating functions formalism for the analysis of spin response to the periodic trains of RF pulses. Echo sequences with arbitrary refocusing angles and resonance offsets, J. Magn. Reson. 196 (2009) 164–169.
[11] V.G. Kiselev, Calculation of diffusion effect for arbitrary pulse sequences, J. Magn. Reson. 164 (2003) 205–211.
[12] H.C. Torrey, Bloch equations with diffusion terms, Phys. Rev. 104 (1956) 563–565.
[13] Y. Zur, An algorithm to calculate the NMR signal of a multi spin-echo sequence with relaxation and spin-diffusion, J. Magn. Reson. 171 (2004) 97–106.
[14] R.F. Busse, A.C.S. Brau, A. Vu, C.R. Michelich, E. Bayram, R. Kijowski, S.B. Reeder, H.A. Rowley, Effects of refocusing flip angle modulation and view ordering in 3D fast spin echo, Magn. Reson. Med. 60 (2008) 640–649.
[15] H.Y. Carr, E.M. Purcell, Effects of diffusion on free precession in nuclear magnetic resonance experiments, Phys. Rev. 94 (1954) 630–638.

[16] S. Meiboom, D. Gill, Modified spin-echo method for measuring nuclear relaxation times, Rev. Sci. Instrum. 29 (1958) 688–691.
[17] J. Hennig, A. Nauerth, H. Friedburg, RARE imaging: a fast imaging method for clinical MR, Magn. Reson. Med. 3 (1986) 823–833.
[18] H.Y. Carr, Steady-state free precession in nuclear magnetic resonance, Phys. Rev. 112 (1958) 1693.
[19] A. Oppelt, R. Graumann, H. Barfuss, H. Fischer, W. Hartl, W. Schajor, FISP: Eine neue schnelle Pulssequenz fuer die Kernspintomographie, Electromedica 54 (1986) 15–18.
[20] D.E. Woessner, Effects of diffusion in nuclear magnetic resonance spin-echo experiments, J. Chem. Phys. 34 (1961) 2057–2061.
[21] R. Courant, D. Hilbert, Methods of Mathematical Physics, vol. 2, Wiley-Interscience, New York, 1989, ISBN 0471504394.
[22] P.J. Basser, J. Mattiello, D. LeBihan, Estimation of the effective self-diffusion tensor from the NMR spin echo, J. Magn. Reson. B 103 (1994) 247–254.
[23] J. Mattiello, P.J. Basser, D. Le Bihan, Analytical expressions for the b matrix in NMR diffusion imaging and spectroscopy, J. Magn. Reson. A 108 (1994) 131–141.
[24] E.O. Stejskal, J.E. Tanner, Spin diffusion measurements – spin echoes in presence of a time-dependent field gradient, J. Chem. Phys. 42 (1965) 288–292.
[25] J.E. Tanner, Use of the stimulated echo in NMR diffusion studies, J. Chem. Phys. 52 (1970) 2523–2526.
[26] M. Weigel, J. Hennig, Contrast behavior and relaxation effects of conventional and hyperecho-turbo spin echo sequences at 1.5 and 3T, Magn. Reson. Med. 55 (2006) 826–835.
[27] M. Weigel, M. Zaitsev, J. Hennig, Inversion recovery prepared turbo spin echo sequences with reduced SAR using smooth transitions between pseudo steady states, Magn. Reson. Med. 57 (2007) 631–637.
[28] D.C. Alsop, The sensitivity of low flip angle RARE imaging, Magn. Reson. Med. 37 (1997) 176–184.
[29] J. Hennig, M. Weigel, K. Scheffler, Multiecho sequences with variable refocusing flip angles: optimization of signal behavior using smooth transitions between pseudo steady states (TRAPS), Magn. Reson. Med. 49 (2003) 527–535.
[30] M. Weigel, J. Hennig, Development and optimization of T2 weighted methods with reduced RF power deposition (Hyperecho-TSE) for magnetic resonance imaging, Z. Med. Phys. 18 (2008) 151–161.
[31] E.L. Hahn, Spin echoes, Phys. Rev. 80 (1950) 580–594.
[32] D. Le Bihan, E. Breton, D. Lallemand, P. Grenier, E. Cabanis, M. Laval-Jeantet, MR imaging of intravoxel incoherent motions: application to diffusion and perfusion in neurologic disorders, Radiology 161 (1986) 401–407.
[33] P. Le Roux, R.S. Hinks, Stabilization of echo amplitudes in FSE sequences, Magn. Reson. Med. 30 (1993) 183–190.
[34] J. Hennig, K. Scheffler, Hyperechoes, Magn. Reson. Med. 46 (2001) 6–12.
[35] R.F. Busse, Reduced RF power without blurring: correcting for modulation of refocusing flip angle in FSE sequences, Magn. Reson. Med. 51 (2004) 1031–1037.
[36] J.P. Mugler, L.L. Wald, J.R. Brookeman, T2-weighted 3D spin-echo train imaging of the brain at 3 Tesla: reduced power deposition using low flip-angle refocusing RF pulses, Proc. Intl. Soc. Magn. Reson. Med. (2001) 438.
[37] J.P. Mugler, H. Meyer, B. Kiefer, Practical implementation of optimized tissue-specific prescribed signal evolutions for improved turbo-spin-echo imaging, Proc. Intl. Soc. Magn. Reson. Med. 11 (2003) 203.
[38] J. Hennig, M. Weigel, K. Scheffler, Calculation of flip angles for echo trains with predefined amplitudes with the extended phase graph (EPG)-algorithm: principles and applications to hyperecho and TRAPS sequences, Magn. Reson. Med. 51 (2004) 68–80.
[39] D.G. Norris, Selective parity RARE imaging, Magn. Reson. Med. 58 (2007) 643–649.
[40] D.G. Norris, P. Börnert, T. Reese, D. Leibfritz, On the application of ultra-fast RARE experiments, Magn. Reson. Med. 27 (1992) 142–164.
[41] D.C. Alsop, Phase insensitive preparation of single-shot RARE: application to diffusion imaging in humans, Magn. Reson. Med. 38 (1997) 527–533.
[42] R. Kaiser, E. Bartholdi, R.R. Ernst, Diffusion and field-gradient effects in NMR fourier spectroscopy, J. Chem. Phys. 60 (1974) 2966–2979.
[43] R.F. Karlicek, I.J. Lowe, A modified pulsed gradient technique for measuring diffusion in the presence of large background gradients, J. Magn. Reson. 37 (1980) 75–91.
[44] V.M. Kenkre, E. Fukushima, D. Sheltraw, Simple solutions of the Torrey–Bloch equations in the NMR study of molecular diffusion, J. Magn. Reson. 128 (1997) 62–69.
[45] J. Hennig, A.C. Schulte, K. Il'Yasov, O. Speck, V. Kiselev, Hyperecho diffusion imaging: a new look at diffusion mechanisms, Proc. Intl. Soc. Magn. Reson. Med. 10 (2002) 433.
[46] L.R. Frank, E.C. Wong, T.T. Liu, R.B. Buxton, Increased diffusion sensitivity with hyperechos, Magn. Reson. Med. 49 (2003) 1098–1105.
[47] M.A. Koch, J. Finsterbusch, Compartment size estimation with double wave vector diffusion-weighted imaging, Magn. Reson. Med. 60 (2008) 90–101.
[48] G. Bodenhausen, R. Freeman, G.A. Morris, A simple pulse sequence for selective excitation in Fourier transform NMR, J. Magn. Reson. 23 (1976) 171–175.
[49] G.A. Morris, R. Freeman, Selective excitation in Fourier transform nuclear magnetic resonance, J. Magn. Reson. 29 (1978) 433–462.
[50] D.S. Novikov, V.G. Kiselev, Transverse NMR relaxation in magnetically heterogeneous media, J. Magn. Reson. 195 (2008) 33–39.
[51] P. Callaghan, C. Eccles, Y. Xia, NMR microscopy of dynamic displacements: *k*-space and *q*-space imaging, J. Phys. E Sci. Instrum. 21 (1988) 820–822.
[52] D.S. Tuch, T.G. Reese, M.R. Wiegell, N. Makris, J.W. Belliveau, V.J. Wedeen, High angular resolution diffusion imaging reveals intravoxel white matter fiber heterogeneity, Magn. Reson. Med. 48 (2002) 577–582.
[53] L.R. Frank, Characterization of anisotropy in high angular resolution diffusion-weighted MRI, Magn. Reson. Med. 47 (2002) 1083–1099.